Semi-Supervised Cloud Detection with Weakly Labeled RGB Aerial Images using Generative Adversarial Networks

Toon Stuyck[1], Axel-Jan Rousseau[2], Mattia Vallerio[1] and Eric Demeester[3]
[1]*BASF Antwerpen, BASF, Antwerpen, Belgium*
[2]*Center for Statistics, Data Science Institute, UHasselt, Diepenbeek, Belgium*
[3]*Department of Mechanical Engineering, ACRO Research Group, KU Leuven, Diepenbeek, Belgium*
{*toon.stuyck, mattia.vallerio*}*@basf.com, axeljan.rousseau@uhasselt.be, eric.demeester@kuleuven.be*

Keywords: Generative Adversarial Networks, Cloud Detection, Structural Similarity, Image Segmentation, Anomaly Detection, Semi-supervised Learning.

Abstract: Despite extensive efforts, it is still very challenging to correctly detect clouds automatically from RGB images. In this paper, an automated and effective cloud detection method is proposed based on a semi-supervised generative adversarial networks that was originally designed for anomaly detection in combination with structural similarity. By only training the networks on cloudless RGB images, the generator network is able to learn the distribution of normal input images and is able to generate realistic and contextually similar images. If an image with clouds is introduced, the network will fail to recreate a realistic and contextually similar image. Using this information combined with the structural similarity index, we are able to automatically and effectively segment anomalies, which in this case are clouds. The proposed method compares favourably to other commonly used cloud detection methods on RGB images.

1 INTRODUCTION

Due to the continuous development of satellite and aerial imagery acquisition technology, the use of these types of images is widely applied in various research fields such as environmental monitoring and protection, geographical surveying, military reconnaissance, agriculture engineering and exploitation of mineral resources. According to (King et al., 2013), clouds cover at least 67% of the earth's surface at any given time, hence many of the available satellite and aerial images will contain clouds. These clouds cover areas of interest on the earth's surface and thus lead to inaccurate analysis and interpretation (Saunders, 1986; Saunders and Kriebel, 1988). The ability to automatically detect clouds is a necessity for many of the aforementioned research fields in order to increase accuracy of following algorithms such as image retrieval (Ferecatu and Boujemaa, 2007; Tao et al., 2009) and image classification (Melgani and Bruzzone, 2004).

Multiple cloud detection methodologies have been proposed, but most of these have been designed for sensors like Advanced Very High Resolution Radiometer (AVHRR) and Moderate Resolution Imaging Spectroradiometer (MODIS). However, for our proposed method, the focus lies on cloud detection based on RGB aerial images. Many of the existing cloud detection methods can be classified in two possible categories: threshold based ones (Zhang and Xiao, 2014) and machine learning based ones (Movia et al., 2016; Ozkan et al., 2018; Xie et al., 2017).

In this paper a cloud detection method based on deep learning using an unsupervised *Generative Adversarial Network (GAN)* in combination with *structural similarity (SSIM)* is proposed. Several studies show that GANs have great potential to address anomaly detection problems. GANs have very recently been used successfully in multiple anomaly detection scenarios such as X-ray screening (Akcay et al., 2018) and in medical imaging (Yang et al., 2021). In the case of cloud detection on aerial images, clouds could be identified as anomalies since they are not desired to be on the image.

The remainder of the paper is organized as follows. Section 2 introduces related work. Section 3 describes the GAN used together with structural similarity which has been used for the automated segmentation of clouds. Section 4 presents the experimental results and comparisons to demonstrate the performance of our proposed method as well as limitations. Section 5 reports final conclusions.

Stuyck, T., Rousseau, A-J., Vallerio, M. and Demeester, E.
Semi-Supervised Cloud Detection with Weakly Labeled RGB Aerial Images using Generative Adversarial Networks.
In *Proceedings of the 11th International Conference on Pattern Recognition Applications and Methods (ICPRAM 2022)*, pages 630-635
ISBN: 978-989-758-549-4; ISSN: 2184-4313
Copyright © 2022 by SCITEPRESS – Science and Technology Publications, Lda. All rights reserved

2 RELATED WORK

A short overview of related work regarding to our proposed method will be presented in this section. The topics reviewed are semi-supervised anomaly detection and cloud detection in aerial RGB images.

Semi-Supervised Anomaly Detection. Two of the most common ways for anomaly detection on weakly labeled data are to use either GANs or Variational Autoencoders (VAEs) (Kiran et al., 2018). Both anomaly detection methods are able to produce labels or scores as outputs. However, if there is a need to locate and segment the anomalies, GANs are more appropriate since VAEs will introduce noise and will have more blurred reconstructions (Dosovitskiy and Brox, 2016). For this reason the focus for the remainder of the paper will be limited to GANs. One of the most important developments in anomaly detection using GAN has been made by (Schlegl et al., 2017). The downside of this work is the fact that it is computationally demanding. Later, (Akçay et al., 2019) investigated an adversarial network with skip-connections which resulted in higher performance regarding prior state-of-the-art.

Cloud Detection in Aerial RGB Images. Many cloud detection methods have been proposed for multi-spectral data (Li et al., 2021; Bréon and Colzy, 1999; Frey et al., 2008; Ackerman et al., 2008). (Ozkan et al., 2018) proposed a deep pyramid network which was enhanced with a pre-trained parameter model at the encoder layer which gave satisfying results. This method works with low-orbit Gokturk-2 and RASAT satellites images. Sadly, these methods do not translate well to cloud detection in RGB images. Only limited work has been done regarding specific algorithms for cloud detection in RGB aerial images. (Chan and Vese, 2001) proposed a model for active contours to detect objects in a given image. This method was not specifically designed with cloud detection in mind, but it is still used in some cases. (Zhang and Xiao, 2014) proposed a progressive refinement scheme which was derived based on observations and statistical results. Other work was not found regarding automated cloud segmentation based on aerial RGB images.

3 METHOD

3.1 Overview of the Method

A novel approach for automated detection and segmentation of clouds on weakly labeled RGB aerial images is proposed using Skip-GANomaly (Akçay et al., 2019). This method uses two competing networks. The first network, called the Generator (G), has the objective to capture the distribution of the input dataset (aerial images without clouds) by identifying relevant features and generating new images. The second network, referred to as the Discriminator (D), has the objective to classify the images generated by the Generator to the correct class (i.e. original vs. generated). A high-level overview of this approach is shown in Fig. 1. Using structural similarity (Wang et al., 2004) local deviations between the input image and the generated features can be captured. This information can be used for the automated detection and segmentation of clouds.

3.2 Anomaly Detection using Skip-GANomaly

(Akçay et al., 2019) proposed an approach using GAN for anomaly detection called Skip-GANomaly which has been used in our proposal. In this method both networks are trained adversarially so that the conceptual model is only trained on normal samples, i.e. aerial images without clouds, but tested on both images with and without clouds. Suppose a set of aerial images denoted as $\mathcal{D} = \{x_i, y_i\}_{i=1}^{N}$, where x_i denotes the i-th aerial image from the possible distribution of images p_x and $y_i \in [0,1]$ denotes whether or not the input image contains clouds. By training only on aerial images without clouds, we expect the model to successfully reconstruct images without clouds, but to fail on aerial images where clouds are present, since the model was never trained for these abnormal images. For this reason we expect a higher loss for the reconstruction of abnormal images. The model was trained using a combination of three different loss functions as proposed in (Akçay et al., 2019).

The first loss function is the *adversarial loss* ($\mathcal{L}_{adv}$) which is given by (1). This loss function has the goal to maximize the reconstruction capability of cloudless input images. This means that the generator G generates an image $\hat{x}$ from an orginal image x which comes from the distribution of all possible images p_x as close as possible to the dataset of cloudless training images while the discriminator tries to classify the different images as original (real) or generated (fake). This function needs to be minimized for G and maximized for D.

$$\mathcal{L}_{adv} = \mathop{\mathbb{E}}_{x \sim p_x} [log\, D(x)] + \mathop{\mathbb{E}}_{x \sim p_x} [log\, (1 - D(\hat{x}))] \quad (1)$$

The second loss function is the *contextual loss* ($\mathcal{L}_{con}$). While the adversarial loss makes sure that realistic images are generated, it does not ensure contextual similarity. This can be guaranteed by the contextual

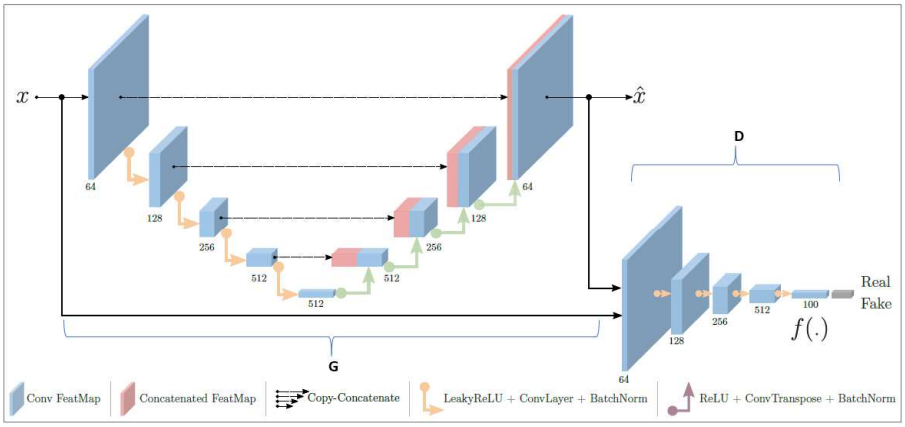

Figure 1: Overview of the proposed generative adversarial network by and taken from (Akçay et al., 2019).

loss which is given in (2), where $|\cdot|_1$ is the L_1 norm. Using the L_1 norm ensures contextual similarity between the original and generated images.

$$\mathcal{L}_{con} = \mathop{\mathbb{E}}_{x\sim p_x} |\, x - \hat{x}\,|_1 \tag{2}$$

The final loss function is the *latent loss* $\mathcal{L}_{lat}$. This loss is defined in (3) and ensures that besides generating realistic images, we can also reconstruct the latent representation of x and $\hat{x}$ as similar as possible. The latent representations of x and $\hat{x}$ are given by $z = f(x)$ and $\hat{z} = f(\hat{x})$.

$$\mathcal{L}_{lat} = \mathop{\mathbb{E}}_{x\sim p_x} |\, f(x) - f(\hat{x})\,|_2 \tag{3}$$

The final training objective is the weighted sum of the losses and is given as:

$$\mathcal{L} = \lambda_{adv}\mathcal{L}_{adv} + \lambda_{con}\mathcal{L}_{con} + \lambda_{lat}\mathcal{L}_{lat}, \tag{4}$$

here λ_{adv}, λ_{con} and λ_{lat} are coefficients to trade off the importance between the three loss terms. Finding the optimal values for these coefficients is a classic multi-objective problem which can be solved using trial and error or by using a multi-objective optimization method (Nimmegeers et al., 2019).

Finally in order to know if clouds are present in the images, an anomaly score has been proposed in (Schlegl et al., 2017). For a given image x, the anomaly score becomes:

$$\mathcal{A}(x) = \lambda R(x) + (1-\lambda)L(x). \tag{5}$$

Here $R(x)$ is the reconstruction score which is based on (2). $L(x)$ is the latent representation score which is based on (3) and λ is a coefficient controlling the importance of the two scoring functions.

3.3 Automated Segmentation using Structural Similarity

Using the architecture explained above, we are able to recreate realistic and contextually similar images compared to the input image. In case we introduce an image with an anomaly (i.e. a cloud) the reconstruction will still be successful except for that part of the image where the anomaly is located. Using this knowledge we can automatically segment the anomalies in the original image x and the generated image $\hat{x}$ using structural similarity (SSIM).

Instead of only looking at absolute differences between pixel values for the comparison, *structural similarity*, as first proposed by (Wang et al., 2004), is based on three components: luminance (l), contrast (c) and structure (s) which are given as:

$$l(x,\hat{x}) = \frac{2\mu_x\mu_{\hat{x}} + c_1}{\mu_x^2 + \mu_{\hat{x}}^2 + c_1}, \tag{6}$$

$$c(x,\hat{x}) = \frac{2\sigma_x\sigma_{\hat{x}} + c_2}{\sigma_x^2 + \sigma_{\hat{x}}^2 + c_2}, \tag{7}$$

$$s(x,\hat{x}) = \frac{\sigma_{x\hat{x}} + c_3}{\sigma_x\sigma_{\hat{x}} + c_3}, \tag{8}$$

with μ_x and $\mu_{\hat{x}}$ the average of x and $\hat{x}$, σ_x^2 and $\sigma_{\hat{x}}^2$ the variance of x and $\hat{x}$, $\sigma_{x\hat{x}}$ the covariance of x and $\hat{x}$ and c_1, c_2 and c_3 variables for stabilization of the division. SSIM is then given as the combination of the three components:

$$SSIM(x,\hat{x}) = l(x,\hat{x}) \cdot c(x,\hat{x}) \cdot s(x,\hat{x}). \tag{9}$$

A SSIM value can be calculated for each pixel using a sliding window. A low SSIM value means a great difference between the two images and thus the presence of an anomaly at the pixel of interest.

4 EXPERIMENTAL RESULTS

The network was trained on a dataset taken from (Srinivas, 2020) which consists of a subset of 1250

aerial images without clouds and validated on a different subset containing 250 cloudless aerial images and 100 aerial images with clouds. The original dataset did not contain ground truth segmentations for the images with clouds. These have been manually segmented by the author. During training this dataset was artificially enlarged using traditional data augmentation techniques, such as flipping, adding noise, cropping, rotation, etc.. Note that in the dataset in the subfolder "noncloud" some images have been manually relabeled, since they were wrongly labeled as noncloud but in fact did contain clouds.

For the training of the network itself, similar parameters as in (Akçay et al., 2019) have been adapted, since they showed these give best overall results. Adam has been used as the optimizer with initial learning rate 0.002 and lambda decay. The momentums are $\beta_1 = 0.5$ and $\beta_1 = 0.999$. The coefficients of the final training objective $\mathcal{L}$ have been set as $\lambda_{adv} = 1$, $\lambda_{rec} = 40$ and $\lambda_{lat} = 1$. The network has been trained three different times, each time with the same parameters, but with a different input image size. The different networks have been trained for images of input size 32×32, 64×64 and 128×128. For every new image to be labeled and if needed segmented, patches of these sizes are taken so that all possible sizes of input images can be used. The results of these different networks for each patch size gets combined in order to obtain more robust automated segmentation of clouds. Each network was trained multiple times for 20 epochs and the best result for each network was selected. Experiments are performed using a PC with an Intel i7-10850h at 2.7 GHz and a NVIDIA Quadro RTX 4000 GPU.

4.1 Comparison with Other Methods

We compare our cloud detection method based on GAN combined with structural similarity with Chan-Vese (Chan and Vese, 2001) and (Zhang and Xiao, 2014). We also wanted to compare our approach with other and more recent approaches. However, as stated in section 2, only limited work has been done regarding specific algorithms for cloud detection in RGB images. Many cloud detection methods for multispectral images exist and give good results, however these do not translate well to cloud detection in RGB images.

Fig. 2, Fig. 3 and Fig. 4 show visual examples of our method compared to the others. White pixels indicate clouds, while black pixels indicate the background. Fig. 2 shows that all methods are good in segmenting individual clear clouds. Fig. 3 shows that in case thin and thick clouds are combined the other

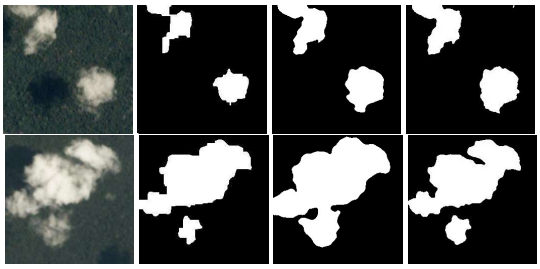

(a) Original image (b) Our method (c) Method by (Zhang and Xiao, 2014) (d) Chan-Vese (Chan and Vese, 2001)

Figure 2: In case of clear clouds and backgrounds, all methods are able to perform good automated segmentation of clouds.

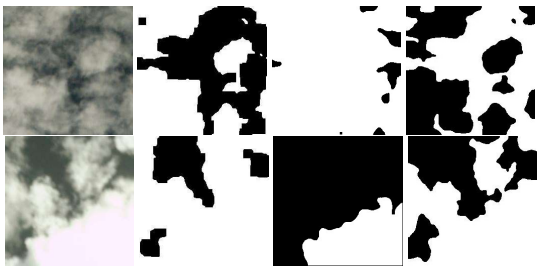

(a) Original image (b) Our method (c) Method by (Zhang and Xiao, 2014) (d) Chan-Vese (Chan and Vese, 2001)

Figure 3: In case most part of the image is covered by clouds (with different transparency) our method outperforms the other two in our validation set.

methods perform worse than ours. Fig. 4 shows results where all methods give poor results. The top original image in this figure contains haze combined with clouds. The bottom original image contains rivers in the background. It appears the training set did not contain enough training images for the G network to learn the complete distribution of possible input images. The generator fails to correctly generate these images leading to misidentification of the river and part of the haze as clouds. (Zhang and Xiao, 2014) proposed method also has difficulties in correctly segmenting the clouds in figure 3 and figure 4. The reason for this is the fact that the method is based on observations and statistics. If there is a lot of variation in the background or many thin, transparent clouds, the method loses part of its robustness.

The Dice coefficient also known as F1-score, defined as follows, is used to numerically quantify our segmentation results:

$$Dice = \frac{2TP}{2TP + FP + FN}, \tag{10}$$

where TP, FP and FN respectively denote the number of true positives, the number of false positives and

Table 1: Quantitative evaluation of different methods on our used dataset.

Method	Dice	ER	Precision	Recall	FAR
Chan-Vese (Chan and Vese, 2001)	0.05	0.51	0.60	0.03	0.40
Method by (Zhang and Xiao, 2014)	0.68	**0.03**	**0.91**	0.65	**0.09**
Our approach	**0.70**	**0.03**	0.78	**0.77**	0.22

(a) Original image (b) Our method (c) Method by (Zhang and Xiao, 2014) (d) Chan-Vese (Chan and Vese, 2001)

Figure 4: In the case haze, or a lot of variation in the background is present all methods have difficulties with segmenting the clouds.

the number of false negatives. Besides the Dice coefficient, four other metrics are used to compare the proposed algorithm with the others. These metrics are the error rate (*ER*), precision, recall and false alarm rate (*FAR*) and are given as:

$$ER = \frac{FP+FN}{\#pixels}, \tag{11}$$

$$precision = \frac{TP}{TP+FP}, \tag{12}$$

$$recall = \frac{TP}{TP+FN}, \tag{13}$$

$$FAR = \frac{FP}{GN}, \tag{14}$$

where $\#pixels$ is the total number of pixels and GN is the number of cloud pixels in ground truth. A good cloud detection method should have high values for precision and recall and low values for ER and FAR. Table 1 shows the evaluation of the metrics on our used dataset for the different cloud detection methods. It is clear that (Zhang and Xiao, 2014) and our method greatly outperform Chan-Vese, and that our proposed method is in general better than (Zhang and Xiao, 2014) expect that it suffers from a higher FAR and thus also has a lower precision.

The fact that our method gets a lower precision and thus also a higher FAR can be brought back to the fact that our training set did not contain enough samples of all possible backgrounds to ensure that our Generator network is able to learn the complete distribution. If a distribution is not completely learned, this will result in a high number of false positives which, according to (12) and (14) will have a negative impact on the precision and FAR metrics.

It should be noted that this paper as well as (Zhang and Xiao, 2014) validated other methods on an own dataset, however both (Zhang and Xiao, 2014) and (Chan and Vese, 2001) scored significantly lower on the dataset used in this paper compared to the reported results of (Zhang and Xiao, 2014). Since we were not able to access the dataset of (Zhang and Xiao, 2014) it is unclear how our dataset and the dataset used in their validation compare to each other.

5 CONCLUSION

In this paper, an effective and robust semi-supervised method is proposed for automated segmentation of clouds on weakly labeled RGB aerial images. The method employs a generative adversarial network for anomaly detection which makes the method invariant to scale and orientation changes. Due to the loss functions used, realistic and contextual similar images are generated except for images that contain anomalies. Using structural similarity combined with this knowledge, the proposed method is able to automatically identify and segment cloud regions. Evaluation shows that the proposed method achieves better performance compared to two other frequently used methods for cloud detection on RGB images, even though our method was never shown images of clouds during training. However, due to the limited training data our generator network was not able to fully learn the distribution of possible input images. This means that our method still suffers from a relatively high false alarm rate. Many of the methods using multi-spectral data are supervised and give good results on this type of data. In general it can be expected that supervised learning leads to better results than semi- or unsupervised learning. However semi- or unsupervised learning might get the preference in the industry since development is less time and effort consuming. Besides this, deep learning methods are also expected to be more robust compared to methods that are based on observations and statistical results. To make sure our expectations are correct, we would like to acquire more training data in order to confirm

that the false alarm rate would decrease and overall Dice score would increase further. In the future, we would like to adapt our work in order to handle different image types, e.g. infrared images as well as the combination of images and depth information. In addition, we would also like to validate this approach for the automated detection and segmentation of foam in a chemical production installation.

ACKNOWLEDGEMENTS

We would like to thank VLAIO and BASF Antwerpen for funding the project (HBC.2020.2876).

REFERENCES

Ackerman, S., Holz, R., Frey, R., Eloranta, E., Maddux, B., and McGill, M. (2008). Cloud detection with modis. part ii: validation. *Journal of Atmospheric and Oceanic Technology*, 25(7):1073–1086.

Akcay, S., Atapour-Abarghouei, A., and Breckon, T. P. (2018). Ganomaly: Semi-supervised anomaly detection via adversarial training. In *Asian conference on computer vision*, pages 622–637. Springer.

Akçay, S., Atapour-Abarghouei, A., and Breckon, T. P. (2019). Skip-ganomaly: Skip connected and adversarially trained encoder-decoder anomaly detection. In *2019 International Joint Conference on Neural Networks (IJCNN)*, pages 1–8. IEEE.

Bréon, F.-M. and Colzy, S. (1999). Cloud detection from the spaceborne polder instrument and validation against surface synoptic observations. *Journal of Applied Meteorology*, 38(6):777–785.

Chan, T. F. and Vese, L. A. (2001). Active contours without edges. *IEEE Transactions on image processing*, 10(2):266–277.

Dosovitskiy, A. and Brox, T. (2016). Generating images with perceptual similarity metrics based on deep networks. *Advances in neural information processing systems*, 29:658–666.

Ferecatu, M. and Boujemaa, N. (2007). Interactive remote-sensing image retrieval using active relevance feedback. *IEEE Transactions on Geoscience and Remote Sensing*, 45(4):818–826.

Frey, R. A., Ackerman, S. A., Liu, Y., Strabala, K. I., Zhang, H., Key, J. R., and Wang, X. (2008). Cloud detection with modis. part i: Improvements in the modis cloud mask for collection 5. *Journal of atmospheric and oceanic technology*, 25(7):1057–1072.

King, M. D., Platnick, S., Menzel, W. P., Ackerman, S. A., and Hubanks, P. A. (2013). Spatial and temporal distribution of clouds observed by modis onboard the terra and aqua satellites. *IEEE transactions on geoscience and remote sensing*, 51(7):3826–3852.

Kiran, B. R., Thomas, D. M., and Parakkal, R. (2018). An overview of deep learning based methods for unsupervised and semi-supervised anomaly detection in videos. *Journal of Imaging*, 4(2):36.

Li, L., Li, X., Jiang, L., Su, X., and Chen, F. (2021). A review on deep learning techniques for cloud detection methodologies and challenges. *Signal, Image and Video Processing*, pages 1–9.

Melgani, F. and Bruzzone, L. (2004). Classification of hyperspectral remote sensing images with support vector machines. *IEEE Transactions on geoscience and remote sensing*, 42(8):1778–1790.

Movia, A., Beinat, A., and Crosilla, F. (2016). Shadow detection and removal in rgb vhr images for land use unsupervised classification. *ISPRS Journal of Photogrammetry and Remote Sensing*, 119:485–495.

Nimmegeers, P., Vallerio, M., Telen, D., Van Impe, J., and Logist, F. (2019). Interactive multi-objective dynamic optimization of bioreactors under parametric uncertainty. *Chemie Ingenieur Technik*, 91(3):349–362.

Ozkan, S., Efendioglu, M., and Demirpolat, C. (2018). Cloud detection from rgb color remote sensing images with deep pyramid networks. In *IGARSS 2018-2018 IEEE International Geoscience and Remote Sensing Symposium*, pages 6939–6942. IEEE.

Saunders, R. (1986). An automated scheme for the removal of cloud contamination from avhrr radiances over western europe. *International Journal of Remote Sensing*, 7(7):867–886.

Saunders, R. W. and Kriebel, K. T. (1988). An improved method for detecting clear sky and cloudy radiances from avhrr data. *International Journal of Remote Sensing*, 9(1):123–150.

Schlegl, T., Seeböck, P., Waldstein, S. M., Schmidt-Erfurth, U., and Langs, G. (2017). Unsupervised anomaly detection with generative adversarial networks to guide marker discovery. In *International conference on information processing in medical imaging*, pages 146–157. Springer.

Srinivas, A. (2020). Cloud and non-cloud images(anomaly detection).

Tao, L., Yuan, L., and Sun, J. (2009). Skyfinder: attribute-based sky image search. *ACM transactions on graphics (TOG)*, 28(3):1–5.

Wang, Z., Bovik, A. C., Sheikh, H. R., and Simoncelli, E. P. (2004). Image quality assessment: from error visibility to structural similarity. *IEEE transactions on image processing*, 13(4):600–612.

Xie, F., Shi, M., Shi, Z., Yin, J., and Zhao, D. (2017). Multilevel cloud detection in remote sensing images based on deep learning. *IEEE Journal of Selected Topics in Applied Earth Observations and Remote Sensing*, 10(8):3631–3640.

Yang, Y., Chen, J., Wang, R., Ma, T., Wang, L., Chen, J., Zheng, W.-S., and Zhang, T. (2021). Towards unbiased covid-19 lesion localisation and segmentation via weakly supervised learning. In *2021 IEEE 18th International Symposium on Biomedical Imaging (ISBI)*, pages 1966–1970. IEEE.

Zhang, Q. and Xiao, C. (2014). Cloud detection of rgb color aerial photographs by progressive refinement scheme. *IEEE Transactions on Geoscience and Remote Sensing*, 52(11):7264–7275.